













Effect of prenatal diaphragmatic hernia on pulmonary arterial morphology

Andrew V. Stainsby^{1,2}  | Philip L. J. DeKoninck^{1,3}  | Kelly J. Crossley^{1,2}  |
 Alison Thiel¹ | Megan J. Wallace^{1,2} | James T. Pearson^{4,5}  |
 Aidan J. Kashyap^{1,2}  | Michelle K. Croughan⁶  | Beth A. Allison^{1,2}  |
 Ryan Hodges^{1,2} | Marta Thio^{7,8} | Andreas W. Flemmer⁹  |
 Erin V. McGillick^{1,2}  | Arjan B. te Pas¹⁰  | Stuart B. Hooper^{1,2}  |
 Marcus J. Kitchen^{1,6} 

¹Ritchie Centre, Hudson Institute of Medical Research, Melbourne, Australia

²Department of Obstetrics and Gynaecology, Monash University, Melbourne, Australia

³Division of Obstetrics and Fetal Medicine, Department of Obstetrics and Gynaecology, Erasmus MC University Medical Center – Sophia Children's Hospital, Rotterdam, The Netherlands

⁴National Cerebral and Cardiovascular Center, Suita, Japan

⁵Department of Physiology, Victoria Heart Institute and Monash Biomedicine Institute, Monash University, Melbourne, Australia

⁶School of Physics and Astronomy, Monash University, Melbourne, Australia

⁷Newborn Research Centre, The Royal Women's Hospital, Melbourne, Australia

⁸The Department of Obstetrics and Gynaecology, The University of Melbourne, Melbourne, Australia

⁹Division of Neonatology Dr. von Hauner Children's Hospital and Perinatal Center, LMU University Hospital, Munich, Germany

¹⁰Division of Neonatology, Department of Pediatrics, Leiden University Medical Center, Leiden, The Netherlands

Correspondence

Stuart B. Hooper, Department of
Obstetrics and Gynaecology, Monash
University, Melbourne Australia.
Email: stuart.hooper@monash.edu

Funding information

Australian Research Council,
Grant/Award Number: FT160100454;
National Health and Medical Research
Council, Grant/Award Numbers:
APP1138049, APP113902, APP1154914;
Victorian Government's Operational
Infrastructure Support Program;
Netherlands Organisation for Health
Research and Development (ZonMw),
Grant/Award Number: NOW-Vidi 2015/
2016

Abstract

Congenital diaphragmatic hernia (CDH) is a major cause of severe lung hypoplasia and pulmonary hypertension in the newborn. While the pulmonary hypertension is thought to result from abnormal vascular development and arterial vasoreactivity, the anatomical changes in vascular development are unclear. We have examined the 3D structure of the pulmonary arterial tree in rabbits with a surgically induced diaphragmatic hernia (DH). Fetal rabbits ($n = 6$) had a left-sided DH created at gestational day 23 (GD23), delivered at GD30, and briefly ventilated; sham-operated litter mates ($n = 5$) acted as controls. At postmortem the pulmonary arteries were filled with a radio-opaque resin before the lungs were scanned using computed tomography (CT). The 3D reconstructed images were analyzed based on vascular branching hierarchy using the software Avizo 2020.2. DH significantly reduced median number of arteries (2,579 (8440) versus 576 (442), $p = .017$), artery

Abbreviations: CDH, congenital diaphragmatic hernia; CT, computed tomography; DH, diaphragmatic hernia; GDn, gestational day n ; PVR, pulmonary vascular resistance; SNP, sodium nitroprusside.

This is an open access article under the terms of the [Creative Commons Attribution-NonCommercial](https://creativecommons.org/licenses/by-nc/4.0/) License, which permits use, distribution and reproduction in any medium, provided the original work is properly cited and is not used for commercial purposes.

© 2023 The Authors. The Anatomical Record published by Wiley Periodicals LLC on behalf of American Association for Anatomy.

numbers per arterial generation, mean total arterial volume (43.5 ± 8.4 vs. $19.9 \pm 3.1 \mu\text{l}$, $p = .020$) and mean total arterial cross-sectional area (82.5 ± 2.3 vs. $28.2 \pm 6.2 \text{ mm}^2$, $p = .036$). Mean arterial radius was increased in DH kittens between the eighth and sixth branching generation and mean arterial length between the sixth and 28th branching generation. A DH in kittens resulted in threefold reduction in pulmonary arterial cross-sectional area, primarily due to reduced arterial branching. Thus, the reduction in arterial cross-sectional area could be a major contributor to pulmonary hypertension infants with CDH.

KEYWORDS

arterial development, computed tomography, congenital diaphragmatic hernia, cross-sectional area, pulmonary arteries

1 | INTRODUCTION

The transition from fetal to newborn life at birth involves a series of changes to the infant's respiratory and cardiovascular systems. Aeration of the lung is the primary trigger for these changes and induces a large decrease in pulmonary vascular resistance (PVR) and increase in pulmonary blood flow (Hooper et al., 2015). In some infants, particularly those born with small, underdeveloped (hypoplastic) lungs, PVR remains high after birth and can result in pulmonary hypertension (PH), which has a high mortality (Kotecha et al., 2012).

Congenital diaphragmatic hernia (CDH) is a condition that can cause lung hypoplasia during fetal development, leading to life-threatening respiratory failure and PH after birth (Kotecha et al., 2012). CDH results from incomplete closure of the diaphragm early in gestation, which allows abdominal contents to herniate into the fetal chest. The displaced abdominal viscera restrict normal lung growth, causing severe lung hypoplasia.

Infants with CDH frequently develop PH after birth and while the precise mechanisms remain unknown, several mechanisms are thought to be involved. These include increased muscularization of small pulmonary arteries and arterioles (Harting, 2017; Mous et al., 2018) and disturbances in the biochemical pathways regulating dilation in the pulmonary vessels (Acker et al., 2015; Keller et al., 2010; Mous et al., 2018). However, there is some debate as to the underlying developmental processes leading to these abnormal pathways, particularly the increased muscularization of pulmonary arteries. Indeed, while elevated arterial pressures are known to increase muscularization of arterial walls (Humphrey, 2008; Wang & Thampatty, 2006), an open ductus arteriosus ensures that pulmonary arterial pressures do not increase during fetal development, no matter how high PVR increases. Thus, the increased muscularization cannot be due to increased

pulmonary arterial pressures. Alternatively, the high PVR in CDH infants may simply be due to the smaller lung size, leading to reduced arterial branching and as a result a reduced summed cross-sectional area of the entire pulmonary vascular bed. On the other hand, establishing lung aeration prior to umbilical cord clamping in lambs with a diaphragmatic hernia (DH) significantly reduces PVR for at least 2 hr after ventilation onset (Kashyap et al., 2019), compared with immediate cord clamping. This indicates that the underlying mechanisms controlling PVR in CDH infants are likely multifactorial and complex. Regardless of the underlying mechanisms, if the pulmonary circulation is anatomically incapable of vasodilating to the point that it can accept the entire output of the right ventricle without a large increase in pressure, then PH must result.

We have used computed tomography (CT) of pulmonary vascular casts to examine the anatomical differences in the pulmonary arterial tree of rabbit kittens with a surgically induced left-sided DH. Our aim was to determine the effect of a DH on pulmonary arterial number, volume, radius, length, cross-sectional area, branching angle, and tortuosity at each arterial generation. Arterial generations are a measure of branching hierarchy, with the right or left main pulmonary artery being designated *Generation 1*. Each time a parent artery bifurcates, the generation of the resulting child arteries is incremented by one. Analysis by generations allows consistent classification of hierarchy without reference to airways or vessel size. Tortuosity is a measure of curvature and is defined as the ratio of the curved length through an artery's centerline to its straight-line end-to-end distance. The cross-sectional area of an artery was defined as the area of a circle with that artery's radius. Branching angle is the smallest angle between two arteries that branch off the same parent artery, with one angle calculated per pair of arteries, beginning at

the second arterial branching generation. We hypothesized that a DH would reduce the number of pulmonary arteries, the arterial volume, radius, length, and the total, summed cross-sectional area, while increasing the branching angle and tortuosity at each generation number.

2 | MATERIALS AND METHODS

2.1 | Animal care and procedures

All animal procedures were approved by the Monash University Animal Ethics Committee and the Australian Synchrotron Animal Ethics Committee. Pregnant New Zealand white rabbits underwent aseptic surgery at 23 days gestational age (GD23) to induce a left-sided DH in up to two fetuses per rabbit as previously described (DH; $n = 7$; Flemmer et al., 2007; Jani et al., 2009). A second group acted as sham-operated controls (control; $n = 7$), again up to two fetuses per rabbit. At GD30, kittens were delivered via cesarean section, intubated, and then ventilated for 10 min via endotracheal tube. Kittens were then euthanized with sodium pentobarbitone ($0.05 \text{ mg } \mu\text{L}^{-1}$ intraperitoneal; Lethabarb, Virbac, New South Wales, Australia).

2.2 | Analysis of pulmonary vasculature

2.2.1 | Microfil infusion and lung tissue collection

Immediately following euthanasia, the kitten's lungs, heart, and trachea were exposed. The right ventricle was punctured with a 22-gauge needle and a polyethylene cannula (internal diameter 0.5 mm, external diameter 0.8 mm; Natsume, catalog number SP31) was inserted through the puncture site into the pulmonary trunk and then secured with a ligature (3–0 Safil[®], B. Braun, Melsungen, Germany). The lungs were then ventilated via the endotracheal tube with a peak inflation pressure of 20 cmH₂O and a positive end-expiratory pressure of 5 cmH₂O using a purpose-built ventilator (Kitchen et al., 2010). The pulmonary circulation was then gently flushed with sodium nitroprusside (SNP; 40 $\mu\text{g ml}^{-1}$; Pfizer Australia, New South Wales, Australia) via the cannula, using a hand-driven syringe to dilate the arteries.

Microfil[™], which is a lead-based silicone polymer, was used as an X-ray imaging contrast agent for the pulmonary arteries. Microfil solidifies after injection into vascular spaces, forming a cast of the vasculature (Phillips et al., 2017). A solution of 4.7 ml of Microfil was

prepared from 2.5 ml Microfil Yellow (Microfil MV-122, Flow Tech Inc., Massachusetts, USA), 2 ml diluent (Microfil MV-Diluent, Flow Tech Inc., Massachusetts, USA) and 0.2 ml curing agent (Microfil MV-Curing Agent, Flow Tech Inc., Massachusetts, USA). After flushing the pulmonary arteries with SNP, Microfil was slowly infused into the pulmonary arteries via the cannula with a 5 ml hand-driven syringe. Microfil infusion was ceased when the small arteries at the surface of the lung were observed filling under a microscope. The Microfil was left to set for at least 30 min. The lungs were then imaged with a 2D chest X-ray to make an initial assessment of the quality of the Microfil penetration.

Once the Microfil had set, the right and left lungs were removed from the thoracic cavity, separated, preserved in 10% formalin (Sigma-Aldrich Inc., Missouri, USA), and then refrigerated for 24 hr. The lungs were then immersed in compound sodium lactate (Baxter International Inc., Illinois, USA) for 2 hr, before being placed in 2% agarose (Sigma-Aldrich Inc., Missouri, USA) to prevent movement artifacts during imaging.

2.2.2 | CT scans

Imaging was performed at the Imaging and Medical Beamline of the Australian Synchrotron. A monochromatic parallel X-ray source tuned to 25 keV was used to acquire the images at an object-to-detector distance of 3.0 m. Each lung was placed in the path of the X-ray beam and rotated 180° while acquiring 2,201 images per lung. The imaging detector was comprised of a 25- μm thick Gadox phosphor ($\text{Gd}_2\text{O}_2\text{S:Tb}$; P43) coupled to a tandem lens system and a $2,560 \times 2,160$ pixel pco.edge 5.5 sCMOS sensor, resulting in an effective pixel size of 16.2 μm . The 2D images were corrected for beam inhomogeneity, detector artifacts, and electrical noise using a pixel-wise correction algorithm (Croton et al., 2018). The beam intensity was normalized with time and a phase retrieval algorithm was applied to enhance the signal-to-noise ratio (Kitchen et al., 2017; Paganin et al., 2002). The images were reconstructed into 3D using a GPU-enabled filtered back-projection reconstruction algorithm in XTRACT (CSIRO; Canberra, Australia).

2.2.3 | Analysis of pulmonary arteries

The software package Avizo 2020.2 (Thermo Fisher Scientific, MA) was used for vascular segmentation, skeletonization, and morphometric analysis of the CT reconstructions.

As the contrast agent rendered the arteries brighter in the CT images, the images were segmented into partitions (artery or nonartery) by defining a brightness

threshold. Segmentation was performed using the Magic Wand tool in Avizo's segmentation editor and involves manually selecting a "seed voxel" before defining a brightness threshold around which to segment. The tool then iteratively selects voxels within the brightness threshold that are adjacent to the seed voxel or another voxel already in the selection. The result is that all arteries bright enough to be detected by imaging are segmented, forming a complete vascular tree.

The segmented volume was then skeletonized in Avizo using the centerline tree skeletonization algorithm, which generates a mathematical graph of the arterial tree. Nodes and edges represent artery intersections and arteries, respectively. Avizo's filament editor was used to edit the skeleton where appropriate, for example, removing aberrant connections. Figure 1 summarizes the image processing from image acquisition to skeletonization.

Avizo measured each artery's length, radius, tortuosity, volume, and branching hierarchy. Data were also extracted from Avizo to calculate arterial branching angle and cross-sectional area using Python 3. The cross-sectional area for all arteries at each generation was summed to yield a cumulative summation of the total cross-sectional area with increasing generation numbers.

Statistical analysis was performed using GraphPad Prism 9.0.1. The total number of arteries per lung, total lung volumes, total arterial cross-sectional area, number of arterial generations, lung weights, body weights, and lung-to-body weight ratios were compared between control and DH groups with unpaired *t* tests (for symmetrically distributed data) or Mann–Whitney *U* tests (for asymmetrically distributed data). Morphometric data were compared using a two-way analysis of variance with arterial generation and group (control vs. DH) as factors. Post hoc comparisons were made between arteries of the same generation using the Šidák test. Left lungs were analyzed both pooled with and separately from right lungs. Statistical significance was defined as a two-tailed *p*-value < .05, and the results are presented as mean ± SEM if symmetrically distributed or median (interquartile range) if asymmetrically distributed.

3 | RESULTS

Seven kittens were allocated to the control group and seven to the DH group. One control kitten developed a natural right-sided CDH and was excluded from the control group. All kittens completed the ventilation protocol, and all 28 lungs were infused with SNP and Microfil. Two lungs from one control kitten were excluded due to poor Microfil infusion quality on the initial 2D chest X-ray. The remaining 26 lungs were imaged at the Australian Synchrotron, reconstructed into 3D, and

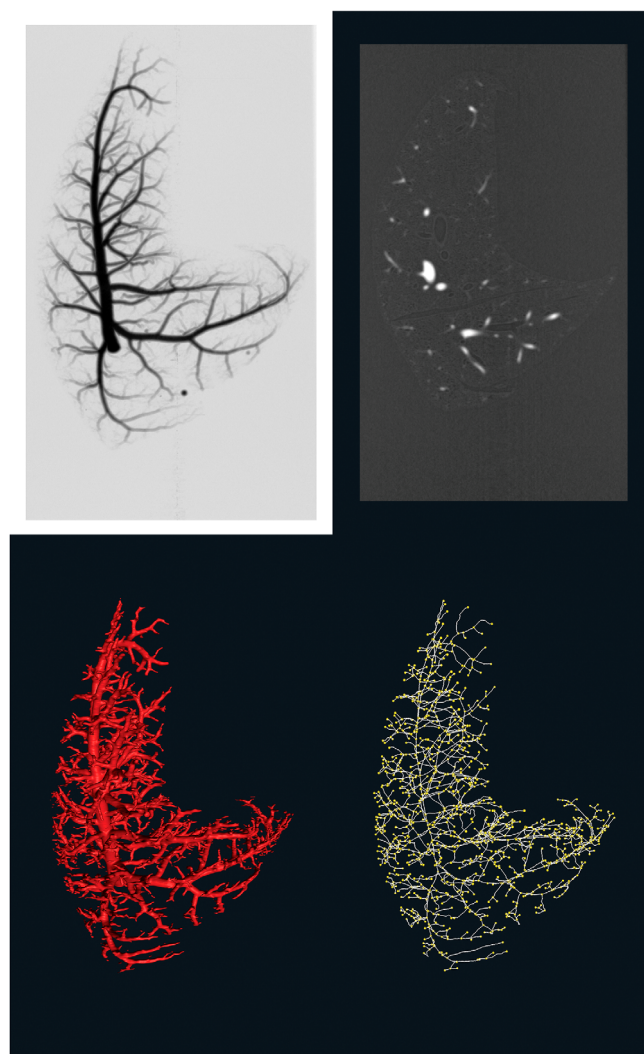
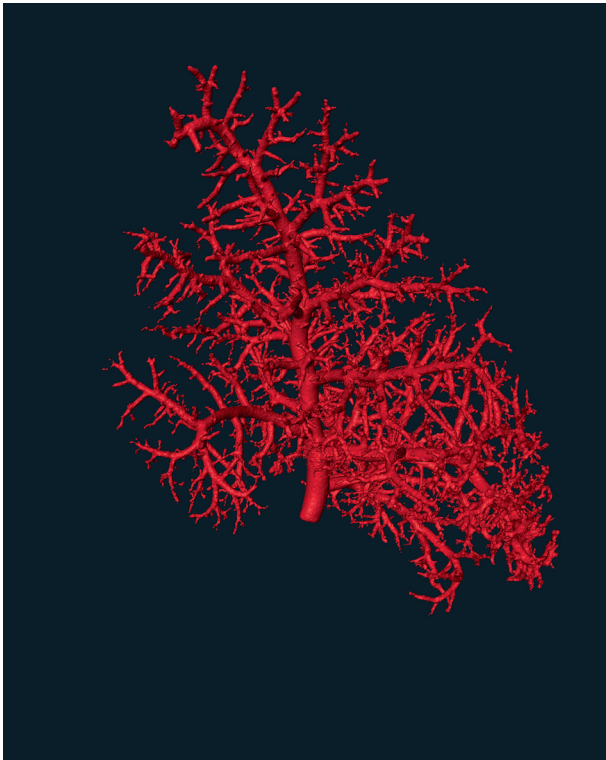


FIGURE 1 Summary of image processing. Top left: a single 2D image acquired during the computed tomography (CT) scan. Top right: a cross-section through the 3D reconstruction of the CT scan. Bottom left: Segmentation of a 3D scan to isolate the arterial tree from other lung structures. Bottom right: skeletonization of the 3D arterial tree to morphometrically analyze the structure by arterial generation number. Gray lines in the skeleton represent arteries, while yellow dots are the intersections between arteries or the endpoints of arteries

segmentation and skeletonization were attempted. Skeletonization was unsuccessful in two lungs from one DH kitten owing to severe arterial rupture not seen on the initial chest X-ray. Segmentation was unsuccessful in the kitten with a natural CDH, so it was not included in the analysis. A total of 10 lungs from 5 control kittens and 12 lungs from six DH kittens were morphometrically analyzed. There were 26,844 arteries between the 22 lungs. All kittens allocated to the DH group had a DH with intrathoracic abdominal viscera confirmed at necropsy. Four of the six DH kittens that were fully analyzed had an at least partially intrathoracic liver.



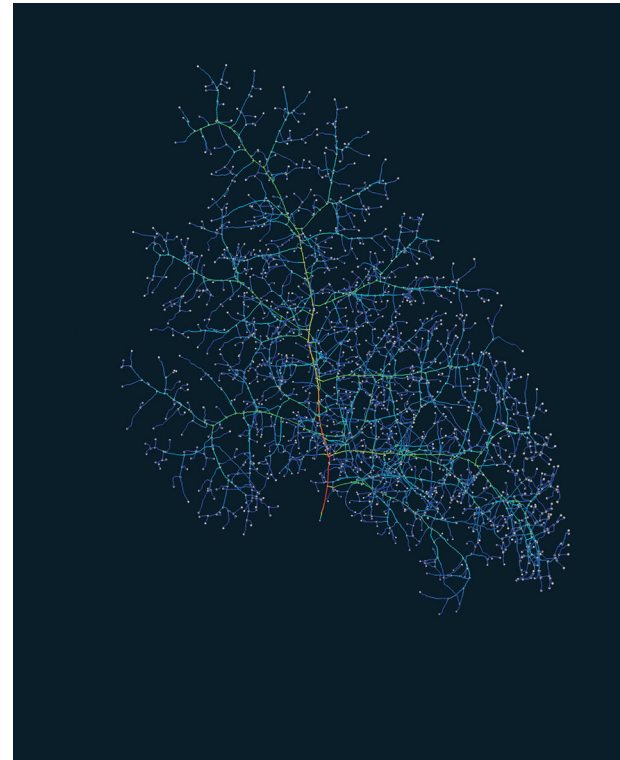
VIDEO 1 A rotating 3D reconstruction of the right pulmonary arterial tree of a control rabbit kitten.

Video content can be viewed at <https://onlinelibrary.wiley.com/doi/10.1002/ar.25159>

Videos 1–4 show representative examples of control and DH pulmonary arterial trees. Videos 1 and 2 are of a control lung's 3D segmentation and skeletonization respectively, whereas Videos 3 and 4 are those of a DH lung. When compared with controls, DH lungs were markedly smaller, had reduced arterial branching and the arterial tree appeared dysmorphic.

3.1 | Whole lung analysis

Total lung weights and both right and left lung weights were significantly lower in DH animals compared with controls (Table 1). Body weight was not different between groups, but lung-to-body weight ratio was markedly reduced in the DH group, indicating lung hypoplasia (Table 1). Similarly, pulmonary arterial volume was significantly lower in DH lungs compared with controls, although when adjusted for lung weight they were similar (Table 1). The total summed cross-sectional area of the pulmonary arterial tree was lower in DH kittens than controls and while this reduction was significant in the right lung, it did not reach statistical significance in the left lungs (Table 1). However, when adjusted for lung weight the total cross-sectional area of the arterial tree



VIDEO 2 A rotating 3D skeleton of a pulmonary arterial tree of a control rabbit kitten. Color Represents vessel thickness from thicker (red) to thinner (blue). The small gray dots are intersections between arteries or arterial endpoints.

Video content can be viewed at <https://onlinelibrary.wiley.com/doi/10.1002/ar.25159>

was similar in control and DH kittens (Table 1). The total number of pulmonary arteries was also lower in the DH group, but this also failed to reach statistical significance in the left lung despite having less than half the median number of arteries (Table 1).

3.2 | Analysis by arterial generation

When analyzed by arterial generation number (Figures 2–5), the numbers of arteries at each generation were markedly reduced in DH kittens, beginning from Generations 7–8, although the difference was not statistically significant until Generation 19 (Figure 2a). Reduced numbers of arteries were evident in both the left and right lungs. Similarly, the cumulative cross-sectional area of the pulmonary arteries was markedly reduced in DH kittens and by Generation 40 was only approximately one-third of that of controls (Figure 2b).

Although arterial radii in DH lungs tended to be smaller for the first couple of generations than controls, the mean radii of middle-generation (10–30) arteries were significantly greater in DH lungs than controls, which



VIDEO 3 A rotating 3D reconstruction of the left pulmonary arterial tree of a rabbit kitten with a left-sided diaphragmatic hernia.

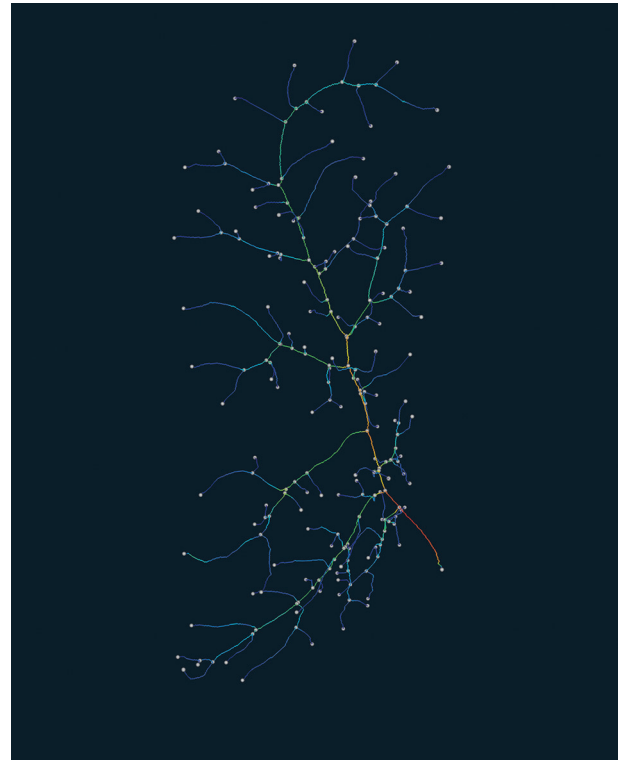
Video content can be viewed at <https://onlinelibrary.wiley.com/doi/10.1002/ar.25159>

was again evident in both left (Figure 3a) and right (Figure 3b) lungs. Mean arterial length for each generation was mostly similar in left lungs of control and DH kittens (Figure 4a), although in the right lung, arterial lengths were significantly increased in DH lungs between Generations 6–28 (Figure 4b).

Branching angles were not different in DH and control lungs (Figure 5a), although tortuosity was reduced in the left lung of DH kittens compared with controls for select generations (Figure 5b).

4 | DISCUSSION

The lung hypoplasia associated with CDH severely compromises respiratory function in the immediate newborn period and commonly leads to the development of severe PH during the first few days after birth (Kotecha et al., 2012). However, the precise mechanisms underlying the development of PH in CDH infants are not well defined and are largely considered to result from abnormal vasoactive responses or to increased muscularization of vessels (Mous et al., 2018). We have examined the 3D structure of the pulmonary arterial trees in rabbit kittens



VIDEO 4 A rotating 3D skeleton of the left pulmonary arterial tree of a kitten with a left-sided diaphragmatic hernia. Color represents vessel thickness from thicker (red) to thinner (blue). The small gray dots are intersections between arteries or arterial endpoints.

Video content can be viewed at <https://onlinelibrary.wiley.com/doi/10.1002/ar.25159>

with severe lung hypoplasia induced by a DH. We found that a surgically induced, left-sided DH caused a severe reduction in lung growth, which included adverse development of the pulmonary vascular tree. The total numbers of arteries were markedly reduced in both the left and right lungs of DH kittens, but while fewer in number the middle generation arteries were on average wider and longer. Nevertheless, total arterial volumes and, in particular, total cross-sectional areas of the arterial tree, were markedly reduced in response to a DH. A pulmonary vascular bed with a large cross-sectional area is a well-established feature of a healthy lung and is required to achieve a PVR that is ~15 times lower than systemic vascular resistance. Thus, a markedly reduced cross-sectional area must result in a persisting high resistance after birth and likely represents an irreversible component of the high PVR in CDH infants. As this component of the high resistance is anatomical, it is unlikely that vasodilators will be able to compensate for this deficit.

The fetal surgery used to induce the DH was performed at GD23, near the end of the pseudoglandular stage (GD8–24) of lung development in rabbits (Wu

TABLE 1 Lung weights, pulmonary arterial volumes, arterial cross-sectional areas, and number of arteries.

	Control (<i>n</i> = 5)	DH (<i>n</i> = 6)	<i>p</i>
Body weight (g)	35 ± 3	34 ± 3	.4793
Lung weight (g)			
Total	0.982 ± 0.115	0.347 ± 0.033	<.001
Left	0.423 ± 0.038	0.149 ± 0.029	<.001
Right	0.585 ± 0.067	0.202 ± 0.014	<.001
Lung: body weight ratio (%)			
Total	2.8 ± 0.18	1.0 ± 0.10	<.0001
Left	1.1 ± 0.07	0.4 ± 0.09	<.0001
Right	1.6 ± 0.11	0.6 ± 0.04	<.0001
Pulmonary arterial volume (μL)			
Total	43.5 ± 8.4	19.9 ± 3.1	.020
Left	16.2 ± 3.4	7.4 ± 1.4	.031
Right	27.3 ± 5.1	12.5 ± 1.8	.016
Weight-adjusted (μL g ⁻¹)			
Total	42.0 ± 6.2	58.7 ± 10.6	.230
Left	37.5 ± 6.5	56.8 ± 14.6	.288
Right	45.4 ± 6.0	62.1 ± 7.8	.134
Pulmonary arterial cross-sectional area (mm ²)			
Total	82.5 ± 23.2	28.2 ± 6.2	.036
Left	30.3 ± 10.3	11.3 ± 3.3	.091
Right	52.3 ± 13.2	16.9 ± 3.0	.019
Weight-adjusted (mm ² g ⁻¹)			
Total	78.3 ± 19.1	83.7 ± 21.0	.855
Left	68.9 ± 22.0	89.9 ± 33.2	.626
Right	85.3 ± 17.3	82.0 ± 13.7	.953
Number of arteries			
Total	2,579 (863, 9,312)	576 (377, 819)	.017[^]
Left	580 (227, 3,995)	210 (116, 403)	.082 [^]
Right	1999 (645, 5,317)	319 (262, 487)	.017[^]
Weight-adjusted (g ⁻¹)			
Total	1857 (1,071, 2,684)	1,407 (1,175, 2,605)	.762 [^]
Left	1,442 (644, 8,809)	1,294 (751, 3,765)	>.999 [^]
Right	3,105 (1,455, 8,010)	1,644 (1,429, 2,309)	.329 [^]

Note: Results are provided for the entire kitten (left and right lungs added together) and separately for left and right lungs. Lung weight-adjusted values are also provided. Results are presented as mean ± SEM for symmetrically distributed data or median (25th percentile, 75th percentile) for asymmetrically distributed data. Circumflex (^) indicates *p*-values were calculated with a Mann-Whitney *U* test due to asymmetrical distribution. Otherwise, *p*-values were calculated with a student's *t* test. Bold *p*-values indicate statistical significance (*p* < .05).

et al., 2000). The presence of abdominal contents in the chest causes fetal lung deflation, which if severe causes fetal lung growth and development to cease (Hooper et al., 1993; Hooper & Harding, 1995). Contralateral lung growth is also affected, as the increased intrathoracic pressure is transmitted across the mediastinum due to a left-to-right mediastinal shift. As such, we would expect development of the airways and vessels to be adversely

affected from approximately GD23. By this stage, the larger airways and accompanying arterial branches will have developed, whereas the smaller more distal airways and arteries continue to develop well beyond this stage (Pringle, 1986). Thus, it is not surprising we found that development of the smaller arteries was most affected by the DH, causing a severe reduction in the number of distal vessels (Video 3 and Figure 2). However, our analysis

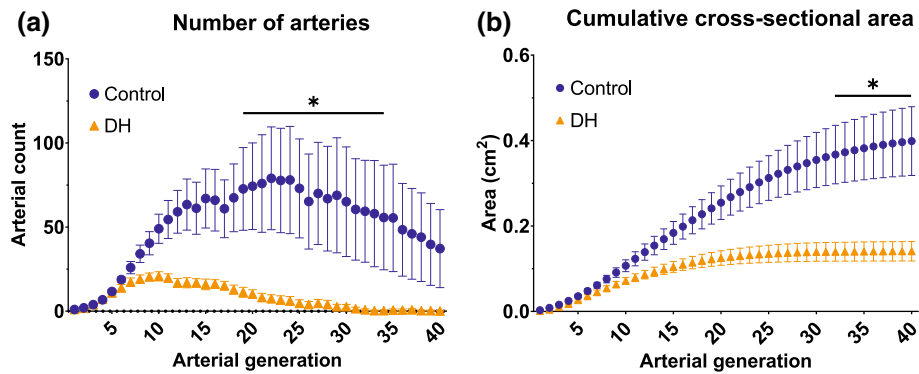


FIGURE 2 (a) Number of pulmonary arteries per lung and (b) cumulative cross-sectional area per lung, analyzed by arterial generation number. Cumulative cross-sectional area is calculated as the summed cross-sectional area of all arteries at the specified generation, plus the cross-sectional area of all arteries belonging to previous arterial generations. Groups shown are control (blue circles, $n = 10$ lungs) and diaphragmatic hernia (DH; orange triangles, $n = 12$ lungs). Data are presented as mean and SEM. Asterisk (*) indicates a significant difference ($p < .05$) between groups at all points below the line

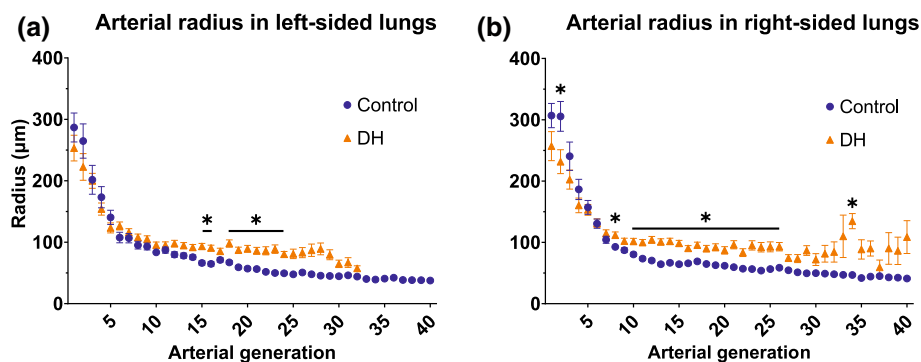


FIGURE 3 Arterial radii in (a) left-sided lungs and (b) right-sided lungs, analyzed by arterial generation number. Groups shown are control (blue circles, $n = 5$ lungs per side) and diaphragmatic hernia (DH; orange triangles, $n = 6$ lungs per side). Data are presented as mean and SEM. Asterisk (*) indicates a significant difference ($p < .05$) between groups at all points below the line, or at the point directly below the asterisk symbol if there is no line

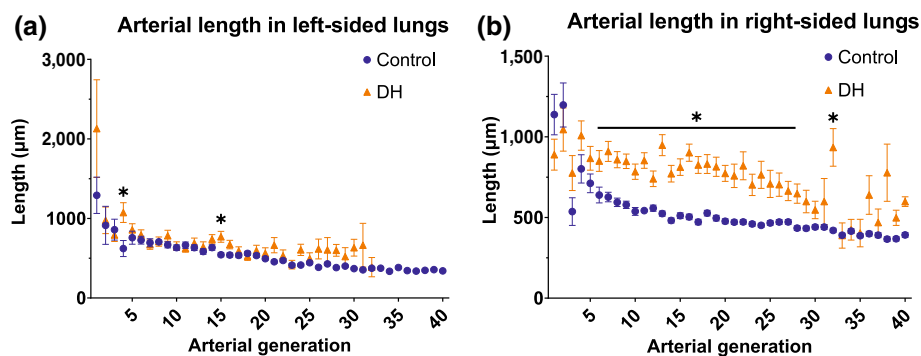
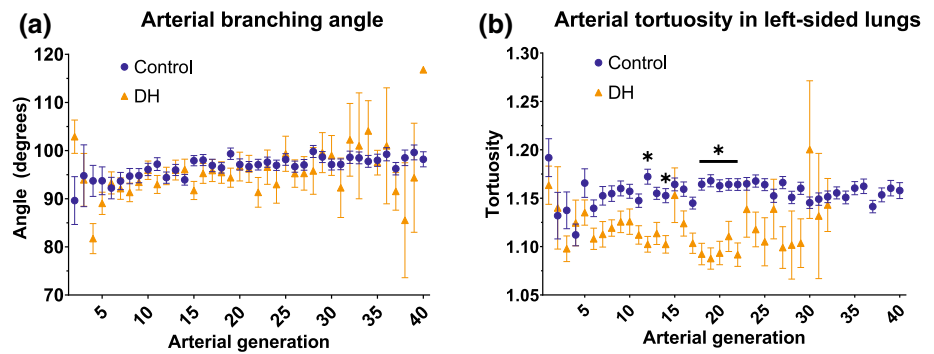


FIGURE 4 Arterial length in (a) left-sided lungs and (b) right-sided lungs analyzed by arterial generation number. Groups shown are control (blue circles, $n = 5$ lungs per side) and diaphragmatic hernia (DH; orange triangles, $n = 6$ lungs per side). Data are presented as mean and SEM. Asterisk (*) indicates a significant difference ($p < .05$) between groups at all points below the line, or at the point directly below the asterisk if there is no line

also found that the number of more proximal vessels (Generations 9–16) were also markedly reduced, despite the expectation that these vessels should have already

developed prior to inducing the DH. This discrepancy can be explained by a reduction in the number of small supernumerary arteries that arise from larger axial

FIGURE 5 (a) Arterial branching angle across all lungs and (b) arterial tortuosity in left-sided lungs analyzed by arterial generation number. Data are presented as mean and SEM. Asterisk (*) indicates a significant difference ($p < .05$) between groups at all points below the line, or at the point directly below the asterisk if there is no line



arteries. These arteries only give rise to a few child generations as they penetrate the nearby lung parenchyma and greatly increase the number of arterial branches compared with the airways (Elliott & Reid, 1965). Nevertheless, as they branch from relatively large arteries, they are classified as a much lower generation number than other arteries of a similar size in our analysis. As a result, a reduction in the number of supernumerary arteries, rather than a reduction in the number of large arterial branches, likely accounts for the reduction in arterial numbers in earlier generations.

A reduction in arterial numbers in DH lungs indicates a severe reduction in arterial branching, which is also consistent with the finding of increased arterial lengths in DH lungs as these were measured between branching points. However, as the increase in arterial length also occurred in lower generation large arteries, it is likely that the reduction/loss of smaller supernumerary arteries that branch off these larger arteries complicates this analysis as well. That is, in control lungs, the presence of smaller supernumerary arteries branching off low-generation large arteries reduces the measured length of the larger arteries. Furthermore, the shorter lengths of the supernumerary arteries are incorporated into the average length measurements of the larger lower generation arteries, skewing the average measurement towards a lower value in control lungs. Similarly, this finding also explains the larger radius observed for any given arterial generation in DH lungs, compared with controls. That is, the smaller radius of the supernumerary arteries will skew the average radius measurement of the larger lower generation arteries towards a lower average measurement in control lungs.

While our measurements of arterial radius at each generation are likely skewed by the reduction in supernumerary arteries in DH lungs, using this model it is not possible for us to determine whether the pulmonary vascular bed in DH lungs was relatively more “vasoconstricted” than controls. This is because these lungs were imaged post-mortem, *ex vivo*, and the pulmonary vascular bed had been dilated with SNP prior to Microfil infusion. Arterial dilation with SNP was performed to achieve better Microfil

penetration. SNP acts directly on arterial smooth muscle to induce dilation, and there is evidence that pulmonary arterial dilation to SNP is not impaired in rabbit kittens with a surgical DH (Schmidt et al., 2013). While the level of arterial dilation may not be strictly reflective of *in vivo* conditions, the objective of this experiment was to examine the anatomical structure, not the physiological capacity to perfuse blood. As such, it is unclear how well the radii measurements reflect *in vivo* conditions, although we would expect the postmortem effects of SNP on pulmonary arterial vessels to be similar in control and DH lungs. Nevertheless, despite a larger average radius, the arterial volume and total cross-sectional area measurements reveal the extent of the arterial tree deficit in DH lungs. In particular, as resistance is inversely proportional to cross-sectional area, the very large decrease in the total cross-sectional area of the pulmonary arterial tree (Figure 2b) must be a major contributor to the high PVR in DH lungs. The significance of this finding is that the deficit is anatomical, which may partially explain why treating PH in CDH infants with vasodilators such as inhaled nitric oxide has little to no effect (Barrington et al., 2017). In control lungs, the arterial generations that provided the greatest contribution to the increase in cross-sectional area, and thus decrease in vascular resistance, are Generations 10–30 (Figure 2b), largely because these generations comprise the vast majority of the pulmonary arteries imaged. However, it is primarily these generations of arteries that are greatly reduced in number or are absent in DH lungs, which accounts for the large reduction in cross-sectional area.

When adjusted for lung weight, the total arterial volume, total cross-sectional area, and total number of arteries are similar in DH and control lungs. Thus, while DH causes a major reduction in arterial growth, this reduction is proportional to the reduction in lung size. This is not surprising given that airway and arterial growth are closely linked during lung development (Gebb & Shannon, 2000; Jakkula et al., 2000), which in turn is driven by mechanical stretch (Hooper & Harding, 1995). *In utero*, the accumulation of liquid within the future

airways causes chronic lung distension, due to the ability of the upper fetal airway to restrict liquid loss from the lungs (Harding & Hooper, 1996). In CDH, migration of abdominal contents into the chest causes lung deflation and a reduction in lung growth by forcing liquid to leave the lungs. As the reduction in arterial growth is proportional to lung size in our DH surgical model, the induced reduction in lung growth is sufficient to explain the reduced arterial development, rather than any independent disturbance to arterial growth.

While the reduction in arterial cross-sectional area in DH lungs was proportional to the reduction in lung size, it is the overall cross-sectional area of the pulmonary arterial tree that determines whether PVR is sufficiently low to prevent PH from developing. This is because, irrespective of the lungs size, 100% of right ventricular output needs to flow through the pulmonary vascular bed, which relies on a high cross-sectional area to maintain a low resistance. If PVR remains high after birth, pulmonary blood flow and pulmonary venous return will remain low, usually resulting in continued right-to-left shunting across the ductus arteriosus. As pulmonary venous return becomes the sole source of preload for the left ventricle after birth (Bhatt et al., 2013), unless right-to-left shunting across the foramen ovale continues, left ventricular output will be diminished (Bhatt et al., 2013).

Our classification of arterial hierarchy into generations provides a simple and unbiased framework to morphometrically analyze the arterial tree at each generation, but it does have limitations. While arteries generally branched into exactly two child arteries, the large axial arteries entering each lobe usually traversed much of the lobe, gradually getting smaller as branches arise from it (see Videos 1 and 2). As such, this approach provided little information on the morphology of these large arteries across their entire length, because each branch was assumed to yield two child generations with the analysis focusing primarily on the inter-branch segments. Furthermore, as explained above, the branching of the smaller supernumerary arteries likely compounded this effect. Nevertheless, this approach provided a simple, unbiased, and robust method for systematically analyzing arterial morphology based on generation number that is applicable to both control and DH lungs.

Another limitation of our study relates to Microfil infusion. Microfil was infused into the pulmonary arteries via hand-driven syringe, so the infusion pressure was not uniform between kittens. The rabbit kittens are very small and the volume of Microfil that entered the pulmonary vascular bed is 10–30 μ l. At this level, an automatic pump is not sufficiently responsive to pressure feedback and there is a risk of transient pressure spikes, even when the pump is set to infuse very slowly. However, infusing

slowly is equally problematic as the Microfil will set within 30 min. While the driving pressure may dilate arteries during Microfil infusion, the pressure returns to atmospheric once the infusion stops, and the elastic recoil of the muscular arterial wall should cause the arteries to contract to their baseline tone. During contraction of the arteries, excess Microfil would be pushed back out of the lung. The endpoint of Microfil infusion, which was the observation of small arteries on the lungs' surface filling under dissecting microscope, was consistent between animals. As such, we do not expect that differences in infusion pressure would lead to variability in data between animals.

The timing of surgical hernia creation in the rabbit model of CDH is likely slightly later than that of natural human CDH. In human CDH, the hernia forms at 10–14 weeks' gestational age, which corresponds to the middle of the pseudoglandular stage (Keller, 2007). In contrast, the hernia is created at the end of the pseudoglandular stage in the surgical rabbit model. During the pseudoglandular stage of lung development, the preacinar airways and blood vessels form, and they are completely developed by the end of this stage. While the hernia forms relatively earlier in humans than in our rabbit model, the impact of the hernia on lung development in humans does not necessarily commence at 10–14 weeks. Although we acknowledge that the hernia could affect lung development to a greater extent in humans than in our rabbit model, the degree of lung hypoplasia seen in humans and in our model are not too dissimilar.

In conclusion, our findings indicate that a large decrease in pulmonary arterial number and cross-sectional area is a major contributor to the high PVR and the onset of PH commonly suffered by CDH infants after birth. We found that a DH causes a major decrease in the number of small, mid-generation arteries which provide the greatest contribution to the large cross-sectional area of the pulmonary arterial tree in control lungs. The reduction in the number of these small, mid-generation arteries not only occurred towards the distal ends of the arterial tree, but also appeared to reduce the number of supernumerary arteries. Finally, as the reduction in pulmonary arterial growth is proportional to the reduction in lung size, antenatal treatments targeted towards increasing lung growth could also have a direct benefit on arterial development in infants with CDH.

AUTHOR CONTRIBUTIONS

Andrew V. Stainsby: Conceptualization; data curation; formal analysis; investigation; methodology; project administration; software; validation; visualization; writing – original

draft; writing – review and editing. **Philip DeKoninck:** Conceptualization; investigation; methodology; writing – review and editing. **Kelly J. Crossley:** Conceptualization; investigation; methodology; writing – review and editing. **Megan Wallace:** Investigation. **James Pearson:** Investigation; methodology; resources; writing – review and editing. **Aidan J. Kashyap:** Investigation; methodology; writing – review and editing. **Alison Thiel:** Investigation; methodology; writing – review and editing. **Michelle Croughan:** Investigation; methodology; software; supervision; writing – review and editing. **Beth Allison:** Supervision; writing – review and editing. **Ryan Hodges:** Conceptualization; writing – review and editing. **Marta Thio:** Investigation; writing – review and editing. **Andreas Flemmer:** Investigation; writing – review and editing. **Arjan te Pas:** Conceptualization; investigation; writing – review and editing. **Stuart B. Hooper:** Conceptualization; funding acquisition; investigation; methodology; project administration; resources; supervision; validation; writing – review and editing. **Erin McGillick:** Conceptualization; data curation; investigation; methodology; project administration; resources; writing – review and editing. **Marcus Kitchen:** Conceptualization; data curation; funding acquisition; investigation; methodology; project administration; resources; supervision; validation; writing – review and editing.

ACKNOWLEDGMENTS

This research was supported by an NHMRC Program Grant (APP113902) and the Victorian Government's Operational Infrastructure Support Program. Stuart B. Hooper was supported by an NHMRC Senior Principal Research Fellowship (APP1154914). Erin V. McGillick was supported by an NHMRC Early Career Fellowship (APP 1138049). ATteP was the recipient of a Vidi grant, The Netherlands Organization for Health Research and Development (ZonMw), part of the Innovational Research Incentives Scheme Veni-Vidi-Vici (NWO-Vidi 2015/2016). Marcus J. Kitchen was supported by an ARC Future Fellowship (FT160100454). The CT scans were performed at the Australian Synchrotron using the Imaging and Medical Beamline facility. Open access publishing facilitated by Monash University, as part of the Wiley - Monash University agreement via the Council of Australian University Librarians.

DATA AVAILABILITY STATEMENT

The data used in this study are available from the corresponding author upon reasonable request.

ORCID

Andrew V. Stainsby  <https://orcid.org/0000-0001-6280-5195>

Philip L. J. DeKoninck  <https://orcid.org/0000-0002-4457-0940>

Kelly J. Crossley  <https://orcid.org/0000-0002-1580-1156>

James T. Pearson  <https://orcid.org/0000-0002-3318-5406>

Aidan J. Kashyap  <https://orcid.org/0000-0003-3587-0535>

Michelle K. Croughan  <https://orcid.org/0000-0001-9345-2345>


Beth A. Allison  <https://orcid.org/0000-0002-1060-513X>

Andreas W. Flemmer  <https://orcid.org/0000-0002-4601-0314>

Erin V. McGillick  <https://orcid.org/0000-0002-9849-5958>

Arjan B. te Pas  <https://orcid.org/0000-0001-7831-8797>

Stuart B. Hooper  <https://orcid.org/0000-0003-1676-4825>

Marcus J. Kitchen  <https://orcid.org/0000-0002-0029-6660>

REFERENCES

- Acker, S. N., Seedorf, G. J., Abman, S. H., Nozik-Grayck, E., Kuhn, K., Partrick, D. A., & Gien, J. (2015). Altered pulmonary artery endothelial-smooth muscle cell interactions in experimental congenital diaphragmatic hernia. *Pediatric Research*, *77*, 511–519.
- Barrington, K. J., Finer, N., Pennaforte, T., & Altit, G. (2017). Nitric oxide for respiratory failure in infants born at or near term. *The Cochrane Database of Systematic Reviews*, *1*, Cd000399.
- Bhatt, S., Alison, B., Wallace, E. M., Crossley, K. J., Gill, A. W., Kluckow, M., Te Pas, A. B., Morley, C. J., Polglase, G. R., & Hooper, S. B. (2013). Delaying cord clamping until ventilation onset improves cardiovascular function at birth in preterm lambs. *The Journal of Physiology*, *591*, 2113–2126.
- Croton, L., Ruben, G., Morgan, K., Paganin, D., & Kitchen, M. (2018). A simple, pixel-wise response correction for ring artifact removal in both absorption and phase contrast X-ray computed tomography. *Optics Express*, *27*, 14231–14245.
- Elliott, F. M., & Reid, L. (1965). Some new facts about the pulmonary artery and its branching pattern. *Clinical Radiology*, *16*, 193–198.
- Flemmer, A. W., Jani, J. C., Bergmann, F., Muensterer, O. J., Gallot, D., Hajek, K., Sugawara, J., Till, H., & Deprest, J. A. (2007). Lung tissue mechanics predict lung hypoplasia in a rabbit model for congenital diaphragmatic hernia. *Pediatric Pulmonology*, *42*, 505–512.
- Gebb, S. A., & Shannon, J. M. (2000). Tissue interactions mediate early events in pulmonary vasculogenesis. *Developmental Dynamics*, *217*, 159–169.
- Harding, R., & Hooper, S. B. (1996). Regulation of lung expansion and lung growth before birth. *Journal of Applied Physiology*, *81*, 209–224.
- Harting, M. T. (2017). Congenital diaphragmatic hernia-associated pulmonary hypertension. *Seminars in Pediatric Surgery*, *26*, 147–153.
- Hooper, S. B., Han, V. K. M., & Harding, R. (1993). Changes in lung expansion alter pulmonary DNA synthesis and IGF-II gene expression in fetal sheep. *American Journal of Physiology*, *265*, L403–L409.

- Hooper, S. B., & Harding, R. (1995). Fetal lung liquid: A major determinant of the growth and functional development of the fetal lung. *Clinical and Experimental Pharmacology & Physiology*, *22*, 235–247.
- Hooper, S. B., te Pas, A. B., Lang, J., van Vonderen, J. J., Roehr, C. C., Kluckow, M., Gill, A. W., Wallace, E. M., & Polglase, G. R. (2015). Cardiovascular transition at birth: A physiological sequence. *Pediatric Research*, *77*, 608–614.
- Humphrey, J. D. (2008). Mechanisms of arterial remodeling in hypertension. *Hypertension*, *52*, 195–200.
- Jakkula, M., Le Cras, T. D., Gebb, S., Hirth, K. P., Tuder, R. M., Voelkel, N. F., & Abman, S. H. (2000). Inhibition of angiogenesis decreases alveolarization in the developing rat lung. *American Journal of Physiology-Lung Cellular and Molecular Physiology*, *279*, L600–L607.
- Jani, J. C., Flemmer, A. W., Bergmann, F., Gallot, D., Roubliova, X., Muensterer, O. J., Hajek, K., & Deprest, J. A. (2009). The effect of fetal tracheal occlusion on lung tissue mechanics and tissue composition. *Pediatric Pulmonology*, *44*, 112–121.
- Kashyap, A. J., Hodges, R. J., Thio, M., Rodgers, K. A., Amberg, B. J., McGillick, E. V., Hooper, S. B., Crossley, K. J., & DeKoninck, P. L. J. (2019). Physiologically based cord clamping improves cardiopulmonary haemodynamics in lambs with a diaphragmatic hernia. *Archives of Disease in Childhood. Fetal and Neonatal Edition*, *105*, 18–25.
- Keller, R. L. (2007). Antenatal and postnatal lung and vascular anatomic and functional studies in congenital diaphragmatic hernia: Implications for clinical management. *American Journal of Medical Genetics Part C: Seminars in Medical Genetics*, *145C*, 184–200.
- Keller, R. L., Tacy, T. A., Hendricks-Munoz, K., Xu, J., Moon-Grady, A. J., Neuhaus, J., Moore, P., Nobuhara, K. K., Hawgood, S., & Fineman, J. R. (2010). Congenital diaphragmatic hernia: Endothelin-1, pulmonary hypertension, and disease severity. *American Journal of Respiratory and Critical Care Medicine*, *182*, 555–561.
- Kitchen, M. J., Buckley, G. A., Gureyev, T. E., Wallace, M. J., Andres-Thio, N., Uesugi, K., Yagi, N., & Hooper, S. B. (2017). CT dose reduction factors in the thousands using X-ray phase contrast. *Scientific Reports*, *7*, 15953.
- Kitchen, M. J., Habib, A., Fouras, A., Dubsky, S., Lewis, R. A., Wallace, M. J., & Hooper, S. B. (2010). A new design for high stability pressure-controlled ventilation for small animal lung imaging. *Journal of Instrumentation*, *5*, T02002.
- Kotecha, S., Barbato, A., Bush, A., Claus, F., Davenport, M., Delacourt, C., Deprest, J., Eber, E., Frenckner, B., Greenough, A., Nicholson, A. G., Antón-Pacheco, J. L., & Midulla, F. (2012). Congenital diaphragmatic hernia. *European Respiratory Journal*, *39*, 820–829.
- Mous, D. S., Kool, H. M., Wijnen, R., Tibboel, D., & Rottier, R. J. (2018). Pulmonary vascular development in congenital diaphragmatic hernia. *European Respiratory Review*, *27*, 170104.
- Paganin, D., Mayo, S. C., Gureyev, T. E., Miller, P. R., & Wilkins, S. W. (2002). Simultaneous phase and amplitude extraction from a single defocused image of a homogeneous object. *Journal of Microscopy*, *206*, 33–40.
- Phillips, M. R., Moore, S. M., Shah, M., Lee, C., Lee, Y. Z., Faber, J. E., & McLean, S. E. (2017). A method for evaluating the murine pulmonary vasculature using micro-computed tomography. *The Journal of Surgical Research*, *207*, 115–122.
- Pringle, K. C. (1986). Human fetal lung development and related animal models. *Clinical Obstetrics and Gynecology*, *29*, 502–513.
- Schmidt, A. F., Rojas-Moscoso, J. A., Gonçalves, F. L., Gallindo, R. M., Mónica, F. Z., Antunes, E., Figueira, R. L., & Sbragia, L. (2013). Increased contractility and impaired relaxation of the left pulmonary artery in a rabbit model of congenital diaphragmatic hernia. *Pediatric Surgery International*, *29*, 489–494.
- Wang, J. H., & Thampatty, B. P. (2006). An introductory review of cell mechanobiology. *Biomechanics and Modeling in Mechanobiology*, *5*, 1–16.
- Wu, J., Yamamoto, H., Gratacos, E., Ge, X., Verbeken, E., Sueishi, K., Hashimoto, S., Vanamo, K., Lerut, T., & Deprest, J. (2000). Lung development following diaphragmatic hernia in the fetal rabbit. *Human Reproduction*, *15*, 2483–2488.

How to cite this article: Stainsby, A. V., DeKoninck, P. L. J., Crossley, K. J., Thiel, A., Wallace, M. J., Pearson, J. T., Kashyap, A. J., Croughan, M. K., Allison, B. A., Hodges, R., Thio, M., Flemmer, A. W., McGillick, E. V., te Pas, A. B., Hooper, S. B., & Kitchen, M. J. (2023). Effect of prenatal diaphragmatic hernia on pulmonary arterial morphology. *The Anatomical Record*, 1–12. <https://doi.org/10.1002/ar.25159>